

Supporting Information

Ir-based electrocatalyst promoted by TME-substituted polyoxovanadate-derived vanadium carbide for efficient hydrogen evolution and oxygen evolution

Pingfan Wu*, Jincheng Li, Zicheng Xiao, Yanchao Zhao, Yu Wang,
Bowen Xiao, and Bo Huang*

^aInstitute of POM-based Materials, Hubei Provincial Key Laboratory of Green Materials for Light Industry, Hubei University of Technology, Wuhan 430068, China,

**Corresponding Author: pingfanwu-111@163.com (P. Wu); huangb2013@126.com (B. Huang)*

Chemicals and measurements

All chemical reagents used in the experiments were purchased from commercial sources without any further purification. The Ir colloid solution was prepared according to the literature.¹ Fourier transform infrared (FT–IR) spectra were measured on a Nicolet iS50 infrared spectrometer using KBr pellets; X-ray diffraction (XRD) patterns were tested on an X-ray diffractometer (Rigaku, D/MAX-TTRIII, 40 KV, 200 mA, Cu K α radiation $\lambda = 0.154178$ nm). X-ray photoelectron spectra (XPS) were tested on an ESCALAB 250Xi equipped with ex situ treatment chamber and the binding energy of C1s (284.5 eV) was used as the reference to correct the measured binding energy. Scanning electron microscopy (SEM) images were obtained on a cold-field emission BUCT. High resolution transmission electron microscopy (HRTEM) images and elemental mapping results were obtained on a Tecnai G2 F20 U-TWIN. UV–Vis spectrum was tested in Shimadzu UV2700 from 800 to 200 nm. Inductively Coupled Plasma Optical Emission Spectroscopy (ICP-OES) is tested on an Agilent ICP-OES730.

Electrochemical tests

The HER and OER activities of different nanoparticles were tested with a standard three-electrode system on a CHI760E electrochemical analyzer (CH Instruments, Inc., Shanghai). All the potentials in this paper were calibrated to the reversible hydrogen electrode (RHE) in 1.0 M KOH according to the following Nernst equation: $E(\text{RHE}) = E(\text{Hg/HgO}) + E^\ominus(\text{Hg/HgO}) + 0.059 \text{ pH}$. In the preparation of a working electrode, 2.0 mg prepared electrocatalyst and 50 μL Nafion solution were dispersed in 150 μL

anhydrous ethanol by ultrasonication for 1 hour to form a homogeneous ink. Then, 5.0 μL of the ink was loaded onto the surface of a glassy carbon electrode (3.0 mm in diameter) and dried at room temperature. Before electrochemical tests, the fresh working electrode was cycled 1,000 cycles to stabilize the current. Linear sweep voltammetry (LSV) was tested in 1.0 M KOH for HER and OER. The Hg/HgO electrode and graphite rod were used as the reference electrode and counter electrode, respectively. Additionally, for the evaluation of C_{dl} value, cyclic voltammograms (CV) were obtained from 0.2 to 0.4 V with sweep rates of 25, 50, 75, 100, 125, 150, 175 and 200 mV s^{-1} . Electrochemical impedance spectroscopy (EIS) was performed at various overpotentials with frequency from 10^{-2} to 10^6 Hz with an AC voltage of 100 mV. All data in the paper are presented without IR compensation.

Preparation of $\text{Na}_2\{\text{V}_6\text{O}_{13}((\text{OCH}_2)_3\text{CCH}_3)_2\}$

The POV precursor of $\text{Na}_2\{\text{V}_6\text{O}_{13}((\text{OCH}_2)_3\text{CCH}_3)_2\}$ was designed and prepared. 1.0 g NaVO_3 dissolved in 20 mL deionized water and then the pH of the solution was adjusted to 2.0 with continuous stirring by dropwise adding 1 M HCl. Later, 0.74 g trimethylolethane (TME) was added additionally to the above solution and the solution was heated to 80°C for 2 days. Finally, the solution was filtrated and red crystals of the product were collected after evaporating the solution in air. The structure was determined by FT–IR and UV–Vis (**Figure S2**). FT–IR spectrum (cm^{-1} , KBr pellets): 514 (w), 580 (w), 618 (w), 711 (m), 791 (m), 950 (vs), 1020 (s), 1129 (m), 1206 (w), 1396 (w), 1455 (m), 1634 (m), 2853 (w), 2898 (w), 3479 (m). UV–Vis

$\lambda_{\max} = 371$ nm.

Preparation of VC/C nanocomposite

Firstly, POV precursor and dicyandiamide with different molar ratio of 1 : 50, 1 : 100, and 1 : 200 (POV : dicyandiamide) were dissolved in deionized water (corresponding to 0.220, 0.110, and 0.055 g Na₂{V₆O₁₃((OCH₂)₃CCH₃)₂} and 1.0 g DCA). The solution was heated at 40 °C in the air to evaporate the water and the red powder was finally obtained. In this case, the POV precursor was successfully incorporated with the carbon source of dicyandiamide. Later, the obtained powder was placed in a porcelain boat and put into the tube furnace. The temperature was heated to 500 °C with a heating rate of 2 °C min⁻¹ for 2 hours, and further raised to 800 °C with a heating rate of 5 °C min⁻¹ for 3 h, then cooled to room temperature. The black powder product of VC/C nanocomposite was washed with deionized water several times then dried by freeze drying. The products were denoted as VC/C-50, VC/C-100, VC/C-200, respectively.

Preparation of Ir colloid solution

The preparation of Ir colloid solution was referred to the reported literature.¹ Typically, 1.0 g IrCl₃·3H₂O was dissolved in 150 mL ethylene glycol under stirring and 0.25 M NaOH ethylene glycol solution was added to adjust the pH value to 10. The mixed solution was heated at 160 °C for 3 hours under flowing Ar, and brown Ir colloid solution (0.292 wt%) can be obtained after cooling to room temperature.

Preparation of Ir/VC/C nanocomposite

50.0 mg pre-prepared VC/C nanocomposite was dispersed in 20 mL ethylene glycol, and then mixed with 5.0 g above Ir colloid solution under stirring for 3 hours. Later, 60 mL deionized water was added into the mixture in twice and continuously stirred for extra 3 hours. The solid sample was collected by centrifuging the mixture and then washed with deionized water for four times. Finally, the solid samples were obtained after freeze drying, and Ir/VC/C nanocomposite was successfully synthesized (denoted as Ir/VC/C-50, Ir/VC/C-100, and Ir/VC/C-200). For comparison, Ir/C was also synthesized through mixing 50.0 mg pre-prepared DCA-derived carbon powder with 5.0 g Ir colloid solution in the above way. The Ir-content in Ir/C is 8.6% and the Ir-content in Ir/VC/C-100 is 10.0%, tested by ICP-OES.

Table S1. Crystal data and structure refinement for Na₂{V₆O₁₃((OCH₂)₃CCH₃)₂}.

Formula	Na ₂ {V ₆ O ₁₃ ((OCH ₂) ₃ CCH ₃) ₂ }
CCDC number	2093050
Empirical formula	C ₁₀ H ₂₂ Na ₂ O ₂₇ V ₆
Formula weight	925.89
Temperature/K	193.0
Crystal system	triclinic
Space group	P-1
a/Å	8.4801(13)
b/Å	8.4744(13)
c/Å	10.9285(17)
α/°	105.368(5)
β/°	101.641(6)
γ/°	94.300(6)
Volume/Å ³	734.8(2)
Z	1
ρ _{calc} g/cm ³	2.092
μ/mm ⁻¹	11.062
F(000)	458.0
Crystal size/mm ³	0.25 × 0.20 × 0.12
Radiation	GaKα ($\lambda = 1.34138$)
2Θ range for data collection/°	12.404 to 121.626
Index ranges	-10 ≤ h ≤ 10, -10 ≤ k ≤ 11, -14 ≤ l ≤ 14
Reflections collected	10169
Independent reflections	3314 [R _{int} = 0.0609, R _{sigma} = 0.0557]
Data/restraints/parameters	3314/0/209
Goodness-of-fit on F ²	1.122
Final R indexes [I>=2σ (I)]	R ₁ = 0.0502, wR ₂ = 0.1449
Final R indexes [all data]	R ₁ = 0.0537, wR ₂ = 0.1486
Largest diff. peak/hole / e Å ⁻³	1.60/-0.87

Table S2. Bond Lengths for Na₂{V₆O₁₃((OCH₂)₃CCH₃)₂}.

Atom	Length/Å	Atom	Length/Å
V1–V2	3.0764(9)	O7–V11	2.032(2)
V1–V3	3.0235(9)	O7–C26	1.439(4)
V1–O5	1.856(3)	O8–C19	1.437(4)
V1–O6	1.600(3)	O10–V11	2.004(3)
V1–O7	2.032(2)	O10–C16	1.445(4)
V1–O10	2.004(3)	O11–V3	1.882(3)
V1–O12	1.812(2)	O13–Na1	2.787(3)
V1–O15	2.2492(6)	O15–V1	2.2492(6)
V2–V3	3.0627(9)	O15–V2	2.2556(6)
V2–O7	1.977(2)	O15–V3	2.2299(6)
V2–O8	2.023(2)	C16–C2	1.532(5)
V2–O11	1.806(3)	C19–C2	1.526(5)
V2–O12	1.874(2)	C26–C2	1.527(5)
V2–O13	1.601(2)	C2–C5	1.539(5)
V2–O15	2.2556(6)	Na1–O13	2.787(3)
V3–V2	3.0627(9)	Na1–Na1	3.486(3)
V3–O5	1.786(2)	Na1–O2	2.340(4)
V3–O8	1.981(2)	Na1–O2	2.434(4)
V3–O10	2.060(2)	Na1–O3	2.375(4)
V3–O11	1.882(3)	Na1–O0AA	2.610(5)
V3–O14	1.608(3)	O2–Na1	2.340(4)
V3–O15	2.2300(6)	O0AA–Na1	2.610(5)
O6–Na1	2.383(3)		

Table S3. Bond Angles for Na₂{V₆O₁₃((OCH₂)₃CCH₃)₂}.

Atom	Angle/°	Atom	Angle/°
V3–V1–V2	64.989(19)	O11–V3–O8	157.37(11)
O5–V1–V2	87.93(8)	O11–V3–O10	84.94(11)
O5–V1–V3	33.15(8)	O11–V3–O15	80.25(8)
O5–V1–O7	86.87(10)	O14–V3–V1	138.16(10)
O5–V1–O10	157.75(11)	O14–V3–V2	135.26(10)
O5–V1–O15	80.38(8)	O14–V3–O5	103.78(13)
O6–V1–V2	137.49(10)	O14–V3–O8	97.91(13)
O6–V1–V3	136.00(10)	O14–V3–O10	96.13(12)
O6–V1–O5	102.89(13)	O14–V3–O11	102.25(13)
O6–V1–O7	97.86(12)	O14–V3–O15	173.06(10)
O6–V1–O10	97.91(13)	O15–V3–V1	47.813(16)
O6–V1–O12	103.69(13)	O15–V3–V2	47.290(17)
O6–V1–O15	173.98(10)	V3–O5–V1	112.23(13)
O7–V1–V2	123.97(7)	V1–O6–Na1	165.40(16)
O7–V1–V3	81.98(7)	V2–O7–V1	110.35(11)
O7–V1–O15	77.16(7)	C26–O7–V1	118.6(2)
O10–V1–V2	81.94(7)	C26–O7–V2	118.8(2)
O10–V1–V3	125.36(7)	V3–O8–V2	109.86(11)
O10–V1–O7	82.54(10)	C19–O8–V2	118.3(2)
O10–V1–O15	78.22(7)	C19–O8–V3	119.3(2)
O12–V1–V2	34.06(8)	V1–O10–V3	108.80(11)
O12–V1–V3	85.78(8)	C16–O10–V1	118.3(2)
O12–V1–O5	92.87(12)	C16–O10–V3	118.2(2)
O12–V1–O7	157.93(11)	V2–O11–V3	112.30(12)
O12–V1–O10	89.76(11)	V1–O12–V2	113.14(13)
O12–V1–O15	81.04(8)	V2–O13–Na1	137.38(15)
O15–V1–V2	47.014(15)	V1–O15–V1	180
O15–V1–V3	47.276(17)	V1–O15–V2	93.85(2)
V3–V2–V1	65.137(19)	V1–O15–V2	86.15(2)
O7–V2–V1	124.72(7)	V1–O15–V2	93.85(2)
O7–V2–V3	81.77(7)	V1–O15–V2	86.15(2)
O7–V2–O8	82.62(10)	V2–O15–V2	180
O7–V2–O15	78.09(7)	V3–O15–V1	84.91(2)
O8–V2–V1	81.02(7)	V3–O15–V1	95.09(2)
O8–V2–V3	123.54(7)	V3–O15–V1	84.91(2)
O8–V2–O15	77.14(7)	V3–O15–V1	95.09(2)
O11–V2–V1	85.64(8)	V3–O15–V2	86.12(2)
O11–V2–V3	34.64(8)	V3–O15–V2	93.88(2)
O11–V2–O7	91.02(11)	V3–O15–V2	93.88(2)
O11–V2–O8	158.18(11)	V3–O15–V2	86.12(2)
O11–V2–O12	92.29(12)	V3–O15–V3	180
O11–V2–O15	81.13(8)	O10–C16–C2	112.6(3)
O12–V2–V1	32.80(8)	O8–C19–C2	111.9(3)
O12–V2–V3	87.91(8)	O7–C26–C2	111.7(3)
O12–V2–O7	156.66(11)	C16–C2–C5	108.5(3)
O12–V2–O8	85.81(11)	C19–C2–C16	110.5(3)
O12–V2–O15	79.61(8)	C19–C2–C26	110.7(3)
O13–V2–V1	135.11(10)	C19–C2–C5	108.5(3)
O13–V2–V3	137.28(10)	C26–C2–C16	109.7(3)

O13–V2–O7	99.42(12)	C26–C2–C5	108.9(3)
O13–V2–O8	98.73(12)	O6–Na1–O13	79.76(10)
O13–V2–O11	102.91(13)	O6–Na1–Na1	145.93(12)
O13–V2–O12	102.34(13)	O6–Na1–O2	161.68(15)
O13–V2–O15	175.36(10)	O6–Na1–O0AA	86.42(12)
O15–V2–V1	46.839(16)	O13–Na1–Na1	80.55(9)
O15–V2–V3	46.588(15)	O2–Na1–O6	104.27(12)
V1–V3–V2	65.46(2)	O2–Na1–O13	77.97(10)
O5–V3–V1	34.63(8)	O2–Na1–O13	88.01(11)
O5–V3–V2	86.47(8)	O2–Na1–Na1	44.17(9)
O5–V3–O8	91.35(11)	O2–Na1–Na1	42.07(9)
O5–V3–O10	159.84(11)	O2–Na1–O2	86.23(13)
O5–V3–O11	93.73(12)	O2–Na1–O3	149.57(14)
O5–V3–O15	82.40(8)	O2–Na1–O0AA	110.87(12)
O8–V3–V1	83.04(7)	O24–Na1–O0AA	76.64(13)
O8–V3–V2	125.67(7)	O3–Na1–O6	97.29(12)
O8–V3–O10	82.77(10)	O3–Na1–O13	127.57(14)
O8–V3–O15	78.59(7)	O3–Na1–Na1	116.74(11)
O10–V3–V1	125.24(7)	O3–Na1–O2	79.35(13)
O10–V3–V2	81.48(7)	O3–Na1–O0AA	83.64(13)
O10–V3–O15	77.55(7)	O0AA–Na1–O13	147.00(12)
O11–V3–V1	88.68(8)	O0AA–Na1–Na1	95.37(12)
O11–V3–V2	33.05(8)	Na1–O2–Na1	93.77(13)

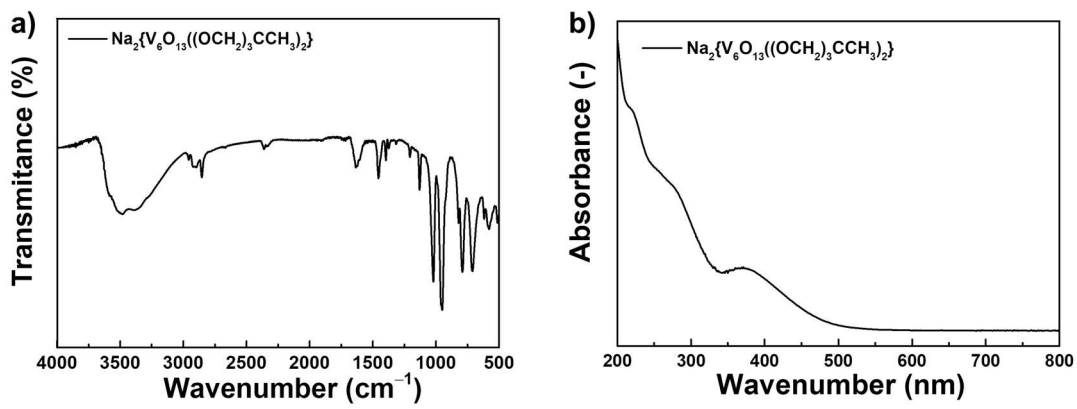


Figure S1. (a) FT–IR spectrum of $\text{Na}_2\{\text{V}_6\text{O}_{13}\text{((OCH}_2)_3\text{CCH}_3\}_2\}$: The peaks near 1020 cm^{-1} and 950 cm^{-1} are attributed to the stretching vibrations of C–O bonds (TME ligand) and V–O_{terminal} bonds (POV core). The stretching vibrations of C–H bonds give signal at 2898 cm^{-1} ; (b) UV–Vis spectrum of $\text{Na}_2\{\text{V}_6\text{O}_{13}\text{((OCH}_2)_3\text{CCH}_3\}_2\}$: The max absorbance peak at 371 nm is V–O_{terminal}.

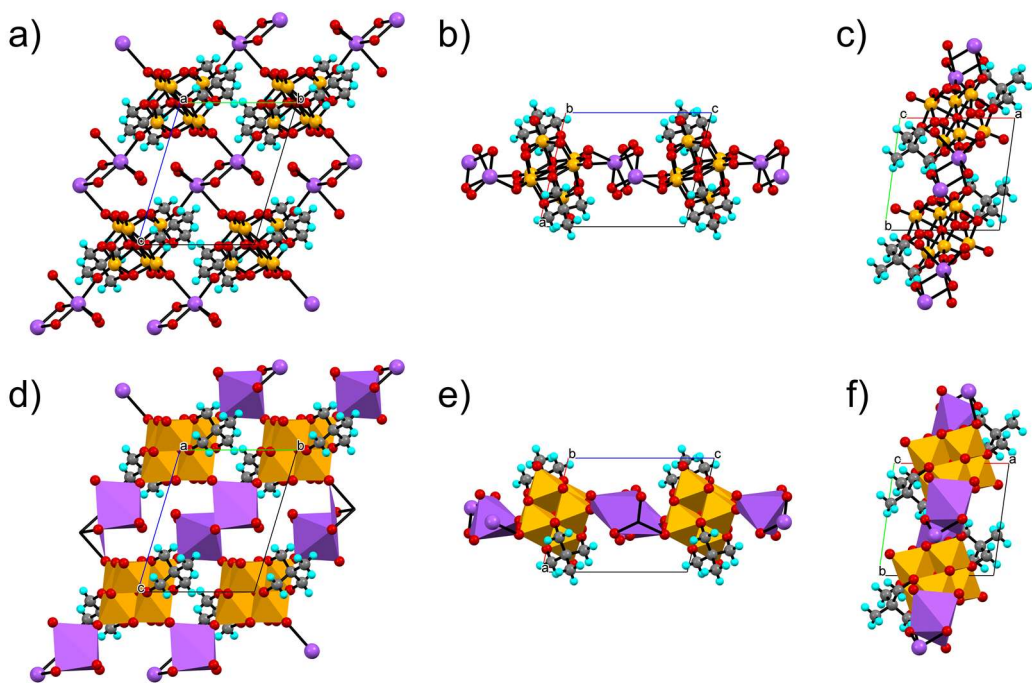


Figure S2. (a–c) Packing diagrams of the obtained POV molecule $\text{Na}_2\{\text{V}_6\text{O}_{13}((\text{OCH}_2)_3\text{CCH}_3)_2\}$ viewed from *a*, *b*, and *c* axis, respectively; (d–f) corresponding polyhedral diagrams viewed from *a*, *b*, and *c* axis, respectively. Yellow sphere: V; red sphere: O; grey sphere: C; light blue sphere: H; purple sphere: Na.

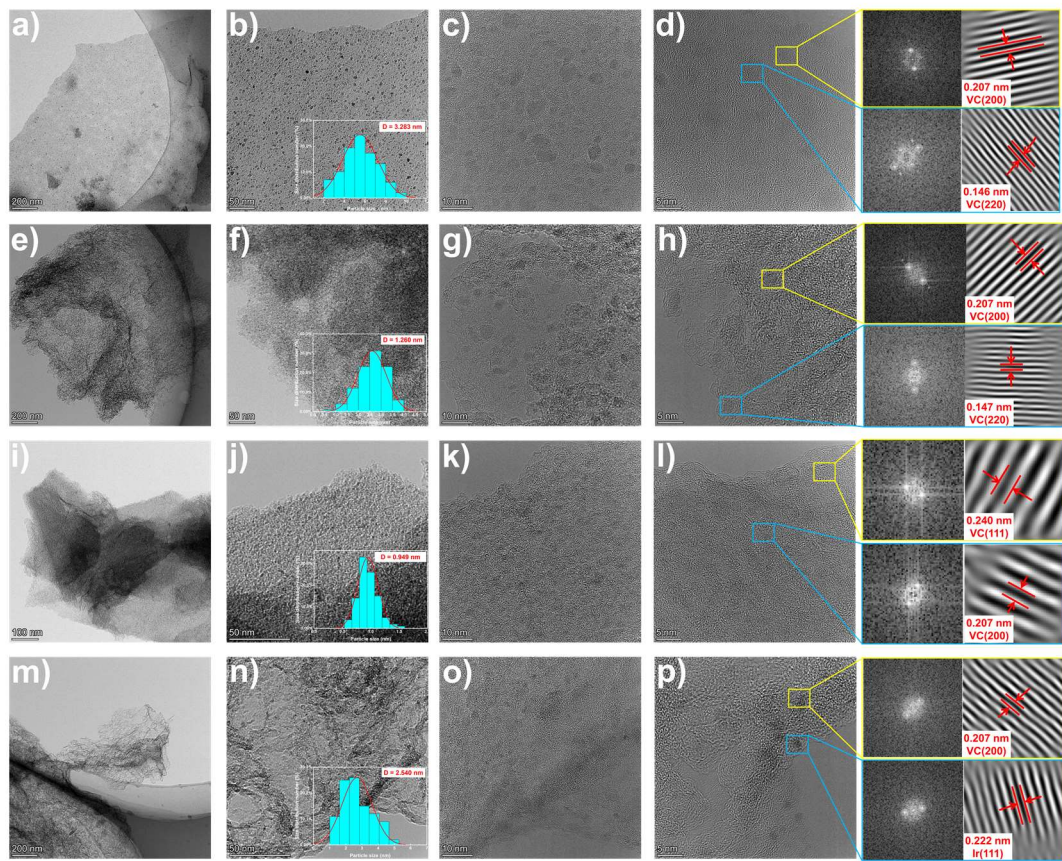


Figure S3. TEM images of VC/C-50 (a–d), VC/C-100 (e–h), VC/C-200 (i–l), and Ir/VC/C-100 (m–p).

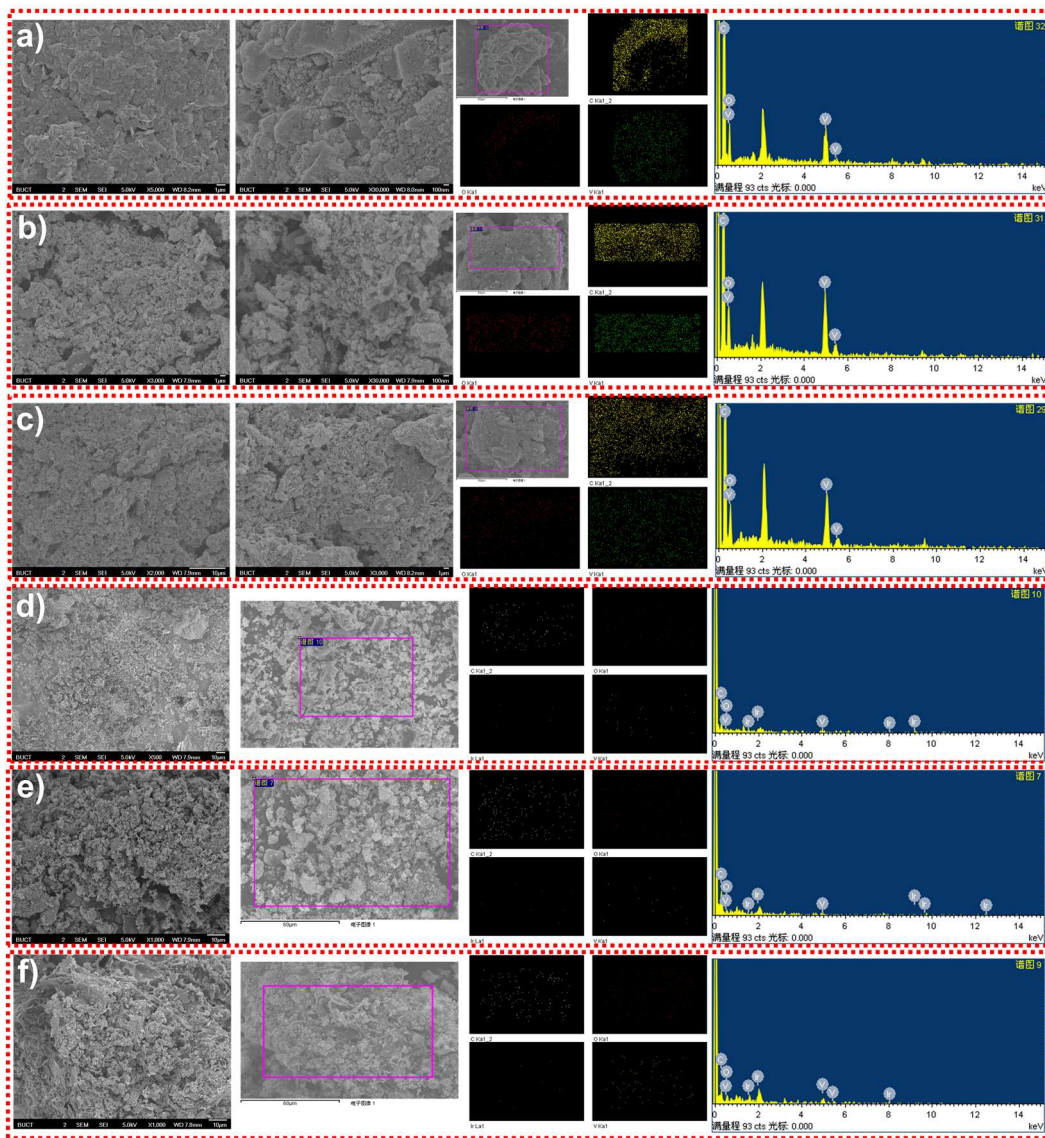


Figure S4. SEM images and EDS mapping results of VC/C-50 (a), VC/C-100 (b), VC/C-200 (c), Ir/VC/C-50 (d), Ir/VC/C-100 (e), and Ir/VC/C-200 (f), respectively.

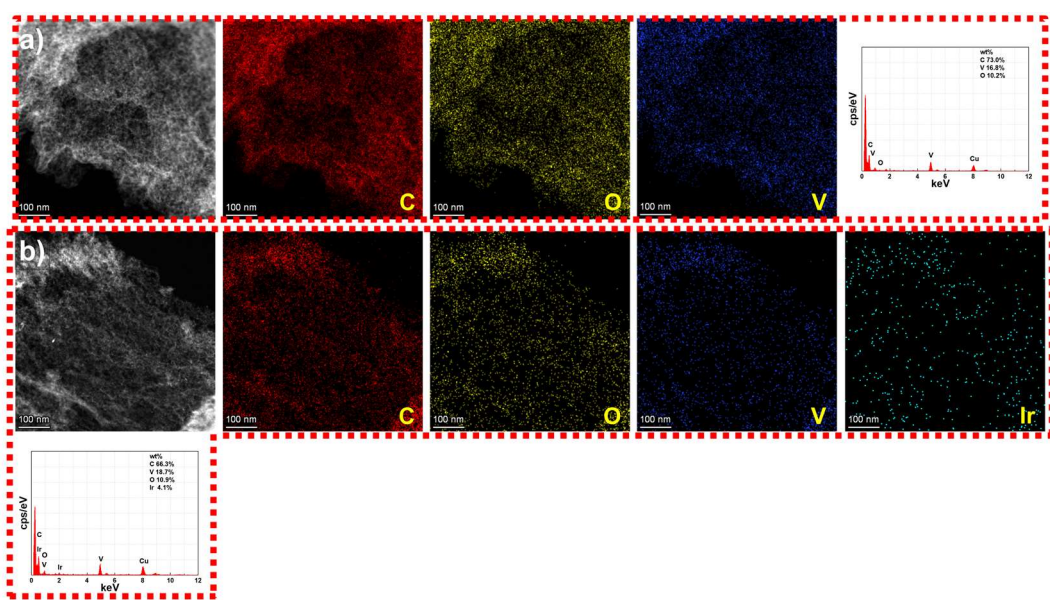


Figure S5. TEM EDS results of VC/C-100 (a) and Ir/VC/C-100 (b).

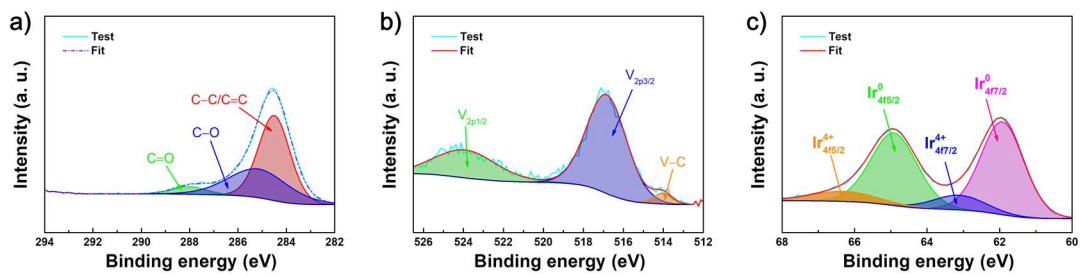


Figure S6. XPS spectra of Ir/VC/C-100 nanocomposite for high resolution spectrum of C1s (a), V2p (b), and Ir4f (c), respectively.

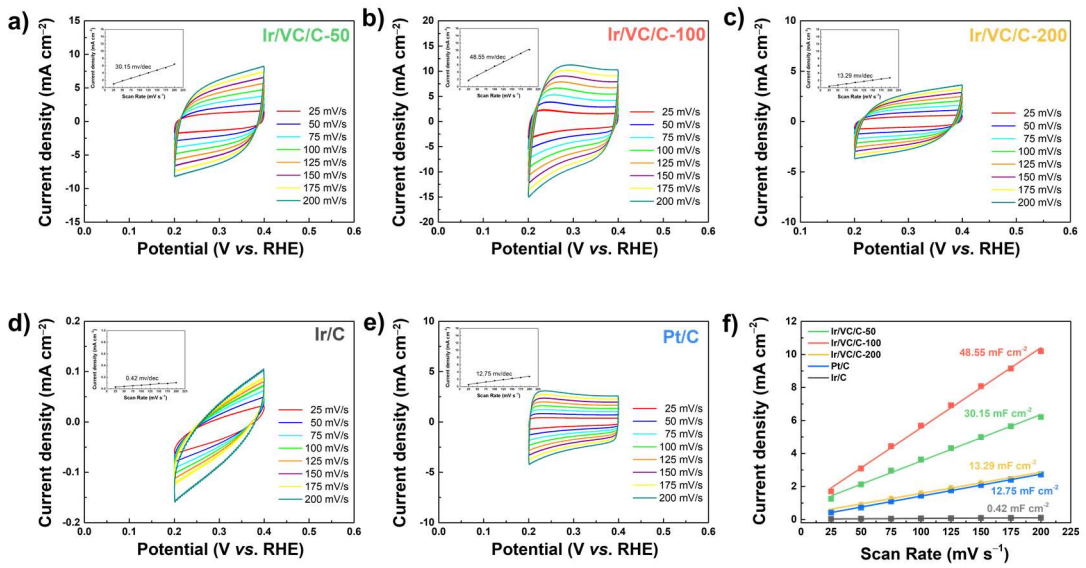


Figure S7. CV curves and the evaluated C_{dl} values of these electrocatalysts of Ir/VC/C, Ir/C, and commercial 20%Pt/C tested in alkaline condition (1.0 M KOH).

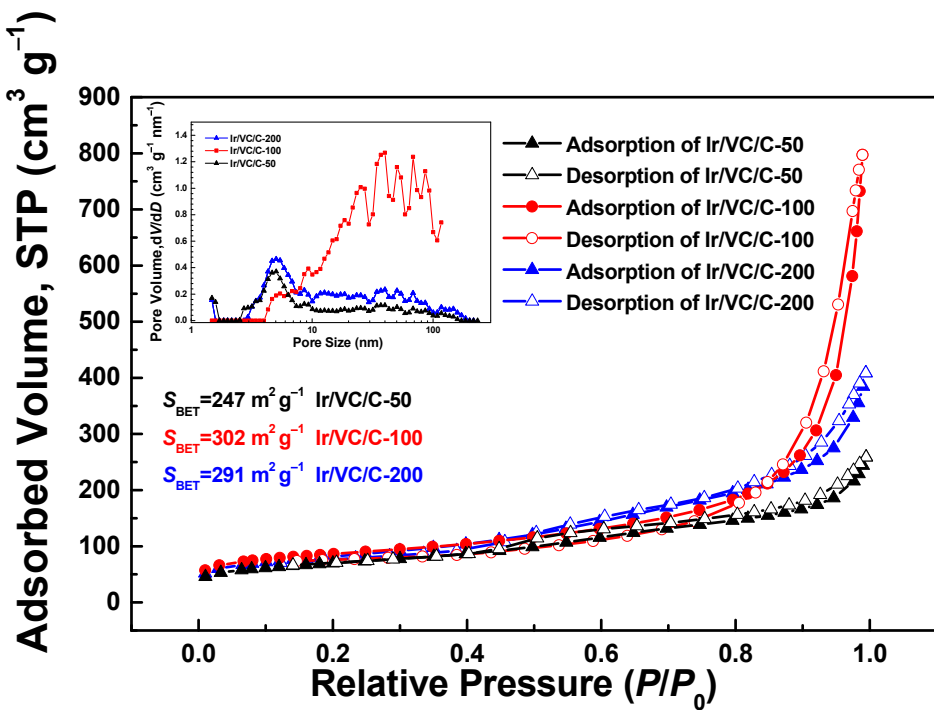


Figure S8. BET specific area results for Ir/VC/C-50, Ir/VC/C-100, and Ir/VC/C-200.

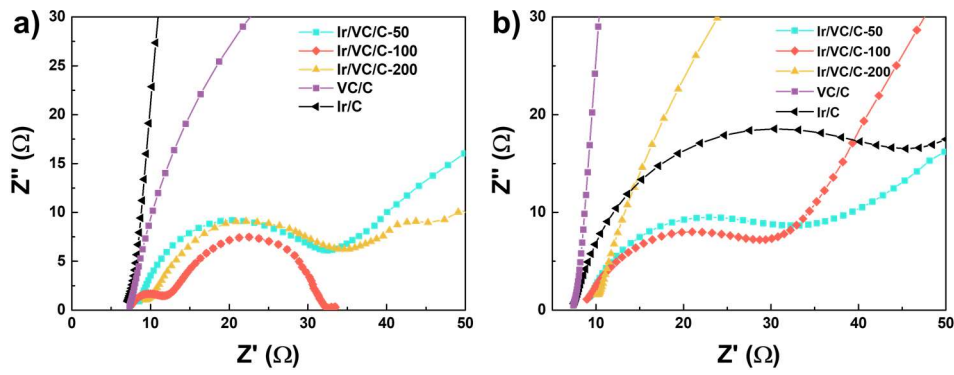


Figure S9. EIS plots of Ir/VC/C, VC/C, and Ir/C nanocomposite tested for HER (a) at 50 mV overpotential and OER (b) at 300 mV overpotential in alkaline condition (1.0 M KOH).

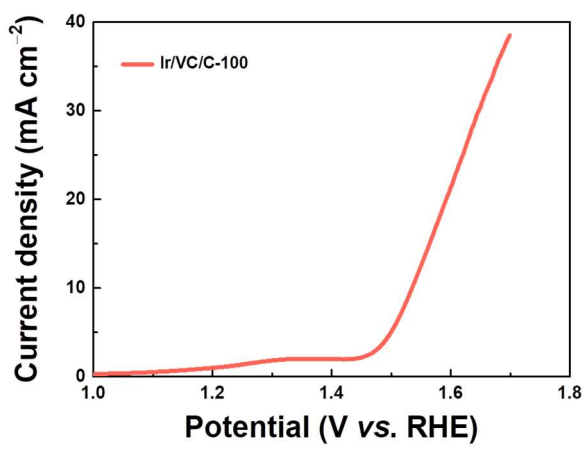


Figure S10. Overall water splitting performance of Ir/VC/C-100.

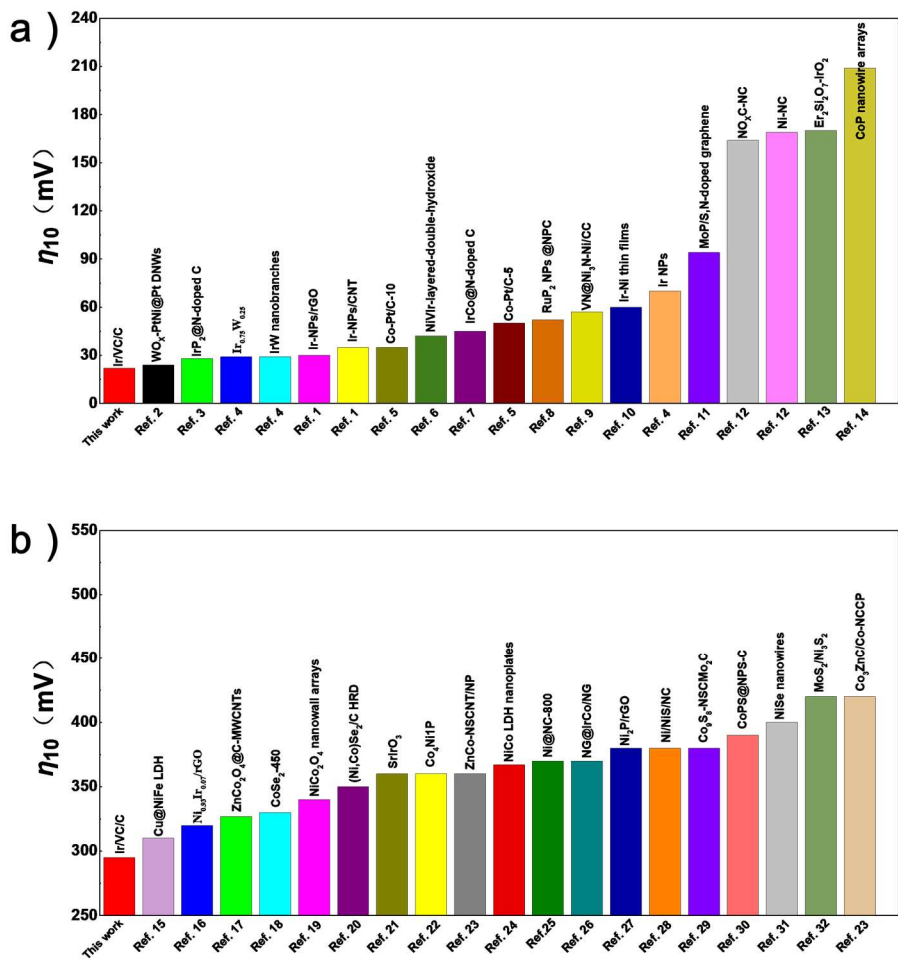


Figure S11. Comparison diagram of η_{10} with other reported cases in alkaline condition (1.0 M KOH) for HER (a)^{1–14} and OER (b).^{15–32}

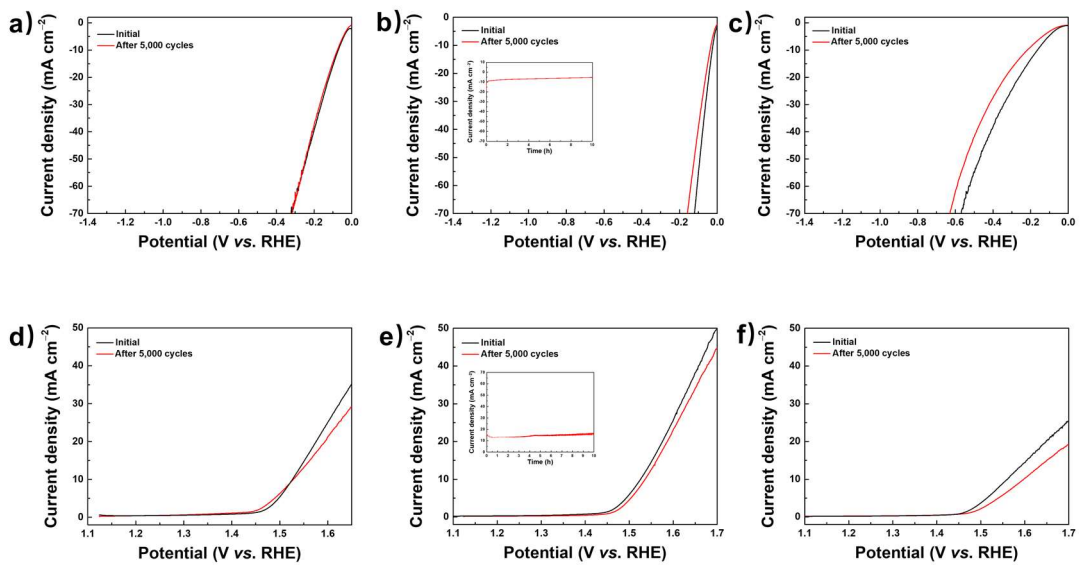


Figure S12. 5,000 cycles durability and electrochemical stability tests of Ir/VC/C-50 (a), Ir/VC/C-100 (b), and Ir/VC/C-200 (c) for HER and Ir/VC/C-50 (d), Ir/VC/C-100 (e), and Ir/VC/C-200 (f) for OER. (insert: 10h i - t test at 10 mA cm^{-2} current density).

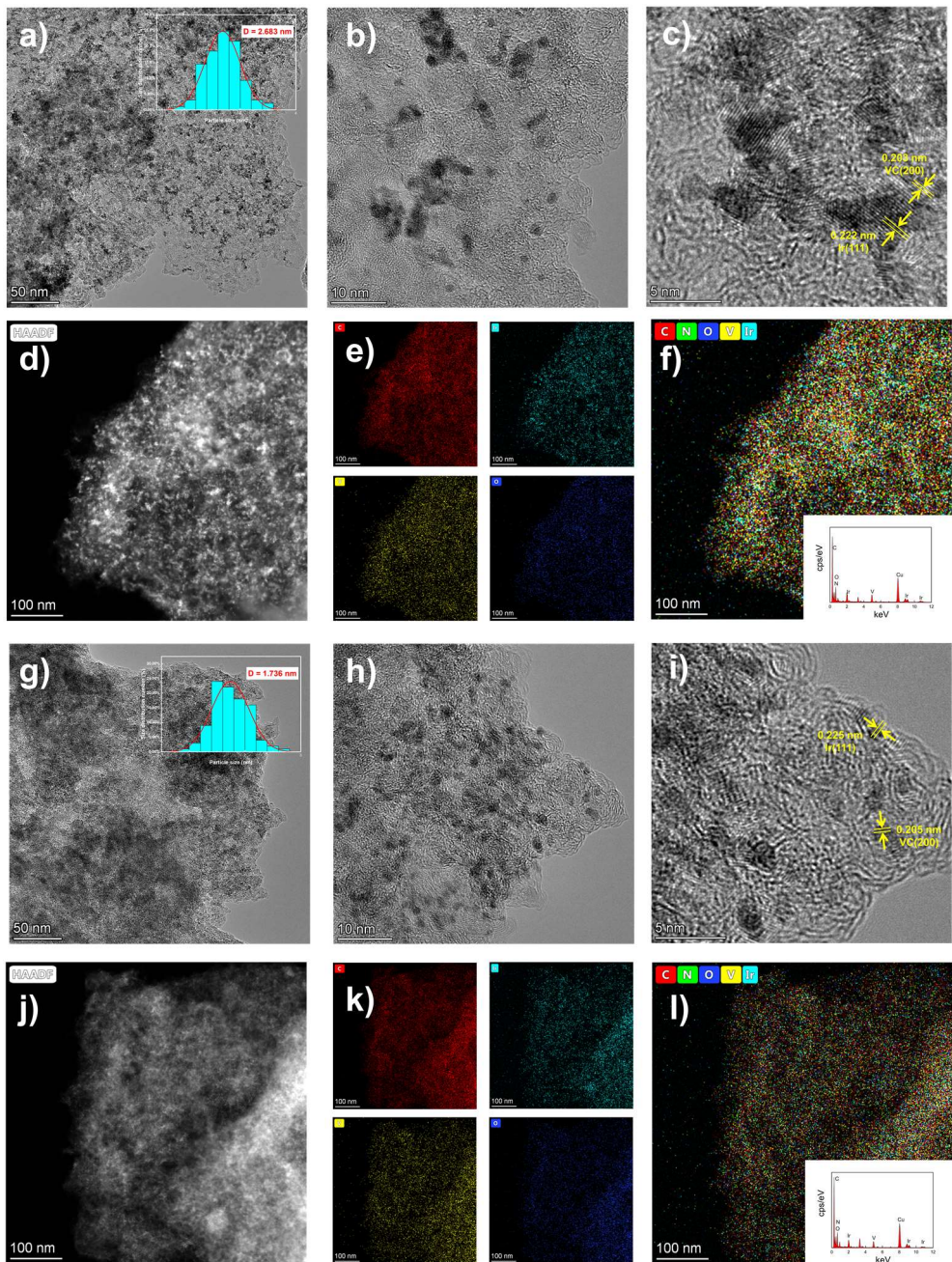


Figure S13. TEM and EDS results of Ir/VC/C-100 for HER(a–g) and OER(h–n) after 5,000 cycle durability tests. the image studies showed following results: 1) the particle size of electrocatalysts after HER and OER test didn't change obviously. After HER, the particle size has tiny aggregation (~2.7 nm), and after OER, the particle size is basically stable (~2.5 nm); 2) the structure of the nanocomposite stays unchanged after long-time cycles and the lattice fringes keep consistent with the X-ray diffraction

clearly: Ir (111) is 0.222 nm and VC (200) is 0.203 nm; 3) the elements are uniformly distributed in the elemental mappings. The above experiment and conclusion demonstrate that Ir/VC/C is a quite stable electrocatalyst for both HER and OER in alkaline condition.

1. B. Huang, Y. T. Ma, Z. L. Xiong, W. D. Lu, R. Ding, T. T. Li, P. Jiang and M. H. Liang, *Sustain. Energ. Fuels*, 2020, **4**, 3288–3292.
2. W. Y. Zhang, B. L. Huang, K. Wang, W. X. Yang, F. Lv, N. Li, Y. G. Chao, P. Zhou, Y. Yang, Y. J. Li, J. H. Zhou, W. S. Zhang, Y. P. Du, D. Su and S. J. Guo, *Adv. Energy Mater.*, 2021, **11**, 2003192.
3. Z. H. Pu, J. H. Zhao, I. S. Amiinu, W. Q. Li, M. Wang, D. P. He and S. C. Mu, *Energy Environ. Sci.*, 2019, **12**, 952–957.
4. L. H. Fu, X. Hu, Y. B. Li, G. Z. Cheng and W. Luo, *Nanoscale*, 2019, **11**, 8898–8905.
5. H. Zhang, Y. Y. Liu, H. J. Wu, W. Zhou, Z. K. Kou, S. J. Pennycook, J. P. Xie, C. Guan and J. Wang, *J. Mater. Chem. A*, 2018, **6**, 20214–20223.
6. S. Li, C. Xi, Y. Z. Jin, D. Y. Wu, T. Liu, H. B. Wang, C. K. Dong, H. Liu, S. A. Kulinich and X. W. Du, *ACS Energy Lett.*, 2019, **4**, 1823–1829.
7. P. Jiang, J. T. Chen, C. L. Wang, K. Yang, S. P. Gong, S. Liu, Z. Y. Lin, M. S. Li, G. L. Xia, Y. Yang, J. W. Su and Q. W. Chen, *Adv. Mater.*, 2018, **30**, 1705324.
8. Z. H. Pu, I. S. Amiinu, Z. K. Kou, W. Q. Li and S. C. Mu, *Angew. Chem. Int. Ed.*, 2017, **56**, 11559–11564.
9. X. Dong, H. J. Yan, Y. Q. Jiao, D. Z. Guo, A. P. Wu, G. C. Yang, X. Shi, C. G. Tian and H. G. Fu, *J. Mater. Chem. A*, 2019, **7**, 15823–15830.
10. W. P. Wu, J. W. Liu, N. Johannes, L. Zhang, Y. Zhang, T. S. Hua and L. Liu, *Catal. Lett.*, 2019, **150**, 1325–1336.
11. M. A. R. Anjum and J. S. Lee, *ACS Catal.*, 2017, **7**, 3030–3038.
12. M. Y. Zhao, K. Li, N. Gong, X. L. Guan, H. W. He, H. Qi, J. H. Peng, W. C. Peng, G. L. Zhang, X. B. Fan, F. B. Zhang and Y. Li, *Int. J. Hydrogen Energ.*, 2020, **45**, 28285–28293.
13. K. Paramita, M. Kartick and M. Rashmi, *ACS Catal.*, 2018, **8**, 8803–8843.
14. J. Q. Tian, Q. Liu, A. M. Asiri and X. P. Sun, *J. Am. Chem. Soc.*, 2014, **21**, 7587–7590.
15. L. Yu, H. Q. Zhou, J. Y. Sun, F. Qin, F. Yu, J. M. Bao, Y. Yu, S. Chen and Z. F. Ren, *Energ. Environ. Sci.*, 2017, **10**, 1820–1827.
16. S. Zhang, X. Zhang, X. R. Shi, F. Zhou, R. H. Wang and X. J. Li, *J. Energ. Chem.*, 2020, **49**, 166–173.
17. J. T. Liu, Y. Xie, Y. Nan, G. L. Gou, X. Z. Li, Y. Y. Fang, X. Wang, Y. Tang, H. D. Yang and J. T. Ma, *Electrochim. Acta*, 2017, **257**, 233–242.
18. X. B. Liu, Y. C. Liu and L. Z. Fan, *J. Mater. Chem. A*, 2017, **5**, 15310–15314.
19. J. L. Liu, D. D. Zhu, T. Ling, A. Vasileff and S. Z. Qiao, *Nano Energy*, 2017, **40**, 264–273.
20. F. W. Ming, H. F. Liang, H. H. Shi, G. Mei, X. Xu and Z. C. Wang, *Electrochim. Acta*, 2017, **250**, 167–173.
21. J. Yu, X. H. Wu, D. Q. Guan, Z. W. Hu, S. C. Weng, H. N. Sun, Y. F. Song, R. Ran, W. Zhou, M. Ni and Z. P. Shao, *Chem. Mater.*, 2020, **32**, 4509–4517.
22. L. T. Yan, L. Cao, P. C. Dai, X. Gu, D. D. Liu, L. J. Li, Y. Wang and X. B. Zhao,

- Adv. Funct. Mater.*, 2017, **27**, 1703455.
- 23. Z. Yu, Y. Bai, S. M. Zhang, Y. X. Liu, N. Q. Zhang and K. N. Sun, *J. Mater. Chem. A*, 2018, **6**, 10441–10446.
 - 24. H. F. Liang, F. Meng, M. Cabán-Acevedo, L. S. Li, A. Forticaux, L. C. Xiu, Z. C. Wang and S. Jin, *Nano Lett.*, 2015, **15**, 1421–1427.
 - 25. Y. Xu, W. G. Tu, B. W. Zhang, S. M. Yin, Y. Z. Huang, M. Kraft and R. Xu, *Adv. Mater.*, 2017, **29**, 1605957.
 - 26. Z. Si, Z. Z. Li, L. H. Lu, M. Y. Liu, Y. Chen, H. Y. Jin, X. C. Tian, K. Dai, J. H. Liu and W. G. Song, *ChemCatChem*, 2019, **11**, 5457–5465.
 - 27. L. T. Yan, H. M. Jiang, Y. L. Xing, Y. Wang, D. D. Liu, X. Gu, P. C. Dai, L. J. Li and X. B. Zhao, *J. Mater. Chem. A*, 2018, **6**, 1682–1691.
 - 28. J. T. Ding, S. Ji, H. Wang, H. G. Gai, F. S. Liu, V. Linkov and R. F. Wang, *Inter. J. Hydrogen Energ.*, 2019, **44**, 2832–2840.
 - 29. X. H. Luo, Q. L. Zhou, S. Du, J. Li, J. W. Zhong, X. L. Deng and Y. L. Liu, *ACS Appl. Mater. Inter.*, 2018, **10**, 22291–22302.
 - 30. Y. P. Hu, F. Li, Y. Long, H. D. Yang, L. L. Gao, X. F. Long, H. G. Hu, N. Xu, J. Jin and J. T. Ma, *J. Mater. Chem. A*, 2018, **6**, 10433–10440.
 - 31. C. Tang, N. Cheng, Z. Pu, W. Xing and X. Sun, *Angew. Chem. Int. Ed. Engl.*, 2015, **54**, 9351–9355.
 - 32. J. Zhang, T. Wang, D. Pohl, B. Rellinghaus, R. Dong, S. Liu, X. Zhuang and X. Feng, *Angew. Chem. Int. Ed. Engl.*, 2016, **55**, 6702–6707.